Impurity scattering of wave packets on a lattice

Wonkee Kim,[1] L. Covaci,[1] and F. Marsiglio[1,2,3]
[1]*Department of Physics, University of Alberta, Edmonton, Alberta, Canada, T6G 2J1*
[2]*DPMC, Université de Genève, 24 Quai Ernest-Ansermet, CH-1211 Genève 4, Switzerland*
[3]*National Institute for Nanotechnology, National Research Council of Canada, Edmonton, Alberta, Canada, T6G 2V4*
(Received 10 April 2006; revised manuscript received 11 September 2006; published 27 November 2006)

Quantum transport in a lattice is distinct from its counterpart in continuum media. Even a free wave packet travels differently in a lattice than in the continuum. We describe quantum scattering in a one-dimensional lattice and illustrate characteristics of quantum transport such as resonant transmission. In particular we examine the transport characteristics of a random trimer model. We demonstrate the real-time propagation of a wave packet and its phase shift due to impurity configurations. Spin-flip scattering is also taken into account in a spin-chain system. We show how individual spins in the chain evolve as a result of a spin-flip interaction between an incoming electron and a spin chain.

DOI: 10.1103/PhysRevB.74.205120 PACS number(s): 72.10.−d, 73.50.Bk, 73.21.Hb

I. INTRODUCTION

In the last few decades the advent of pump-probe optical methods [1–3] and similar measurement techniques has stimulated interest in time-dependent phenomena in physical systems.[4] For example, questions concerning the details of magnetization reversal in ferromagnetic thin films can be addressed experimentally[5] and theoretically.[6] Another example is polaron formation in a semiconductor, where both experimental and theoretical work are just starting.[7] While much of the work on magnetization reversal has utilized a classical or at most semiclassical description,[8–13] more recent work has focused on a fully quantum mechanical description.[14] Such a microscopic description is expected to be necessary and insightful for small (i.e., quantum dot) systems.

Insofar as many of these phenomena occur in the solid state, the underlying lattice structure may play an important role. Concerning the theoretical description of magnetization reversal, calculations to date either have focused on simple models,[8–11,15] or have tried to utilize realistic transport equations with band structures relevant to the materials of interest.[16] In this work we wish to solve simple scattering models based on tight-binding band structures. While we will consider mainly scalar potential scattering, the formalism is extendable to spin-flip scattering, which will be discussed. In particular, an incoming electron can scatter off a ferromagnetic thin film modeled by a Heisenberg Hamiltonian, and we can monitor the real-time reaction of the magnetization to the onslaught of electrons with a completely quantum mechanical description. We also want to utilize a framework that is amenable to numerical calculation. By this we mean the following: as interactions are introduced, problems will become formidable by analytical means and large-scale computation will be required. Most often this means Monte Carlo methods (at least this is so in equilibrium and linear response calculations so far) which are often well suited to simple lattices. For these reasons we believe it is beneficial to have a lattice-based framework to tackle nonequilibrium phenomena in solid state systems.

We begin with a description of the noninteracting electron, where already a different property emerges due to the lattice: the degree of spreading of a propagating wave packet can be controlled by judicious choice of the electron energy. This is always true in one dimension and has more limited validity in higher dimensions. We outline the methodology to solve the problem numerically, and use some illustrative examples to demonstrate the accuracy and efficiency of these calculations. Finally, we discuss spin-flip scattering in a spin chain.

This paper is organized as follows. In Sec. II, we describe wave packet transport in a lattice, and a possible solitonic behavior which is impossible in the continuum limit. Using an example, we also demonstrate the equivalence between the wave packet approach and the usual plane wave approach. In Sec. III, we examine the robustness of the resonance for randomly distributed trimers as their number increases. A direct diagonalization of the Hamiltonian will illustrate the time evolution of a wave packet in a lattice with embedded impurities in Sec. IV. In Sec. V, we briefly explain a procedure to study spin-flip scattering on a lattice. In Sec. VI we summarize our results and outline possible future directions.

II. WAVE PACKET TRANSPORT

In order to understand the differences between calculations of quantum mechanical phenomena in a lattice with their counterpart in the continuum limit, it is appropriate to begin with transport of a free wave packet. As is normally done in textbooks,[17] one can introduce a free Gaussian wave packet in the continuum limit:

$$\psi(x,0) = \frac{1}{(2\pi\alpha^2)^{1/4}} e^{-(1/4)(x-x_0)^2/\alpha^2 + ik_0(x-x_0)} \qquad (1)$$

where x_0 and k_0 are the mean position and momentum, respectively, of the wave packet, and α is the position uncertainty associated with the wave packet. To see the time evolution of the wave packet we expand $\psi(x,0)$ in terms of the momentum eigenstates $|k\rangle$. They are the known solutions to the Schrödinger equation in free space; hence the time-dependent Schrödinger equation is readily solved in this basis. The result is[17]

$$\psi(x,t) = \left(\frac{\alpha^2}{2\pi}\right)^{1/4} \frac{e^{i(k_0 x - E_0 t)}}{\sqrt{\alpha^2 + it/2m}} e^{-(1/4)(x - v_0 t)^2/(\alpha^2 + it/2m)} \quad (2)$$

where $E_0 = k_0^2/2m$ and $v_0 = k_0/m$ are the average energy and particle velocity, respectively. Since $\langle x \rangle = v_0 t$ and $\langle x^2 \rangle = (v_0 t)^2 + [\alpha^2 + (t/2m\alpha)^2]$, the position uncertainty Δx defined as $(\Delta x)^2 = \langle x^2 \rangle - \langle x \rangle^2$ becomes $\Delta x = \sqrt{\alpha^2 + t^2/(2m\alpha)^2}$. Similarly, we obtain the momentum uncertainty $\Delta k = 1/(2\alpha)$. The uncertainty relation is therefore

$$\Delta x \Delta k = \frac{1}{2}\sqrt{1 + \left(\frac{t}{2m\alpha^2}\right)^2}. \quad (3)$$

This means that the uncertainty relation increases as a function of time. Also note that the relation does not depend on the mean momentum of the wave packet; as we will see, this is true only for a parabolic energy dispersion.

In a one-dimensional lattice described by a nearest neighbor tight-binding model, $E_k = -2t_0 \cos(ka)$, where t_0 is the hopping amplitude to the nearest neighbor site and a is the lattice constant. Hereafter we set $a = 1$ and use it as the unit of length. The position is now discrete and represented by x_i, with i the lattice site label. Upon expanding in terms of the momentum eigenstates in a box with periodic boundary conditions, one obtains

$$\psi(x_i,t) = \left(\frac{\alpha^2}{2\pi^3}\right)^{1/4} \int_{-\pi}^{\pi} dk\, e^{ikx_i - \alpha^2(k - k_0)^2 - iE_k t}. \quad (4)$$

Note that the integration is over the Brillouin zone, due to the discreteness of the lattice; nonetheless, if α is large enough, the integration range can be extended from $-\infty$ to ∞ without altering the integral. In the same way, using a large-α expansion for the exponent in Eq. (4), and keeping terms up to $\mathcal{O}(1/\alpha^2)$, one can convert the integral into a Gaussian integral, as in the continuum limit. Performing the integration, we obtain

$$\psi(x_i,t) = \left(\frac{\alpha^2}{2\pi^3}\right)^{1/4} \frac{\sqrt{\pi}}{\sqrt{\alpha^2 + itE''_{k_0}/2}} \times e^{ik_0 x_i - iE_{k_0} t} e^{-(1/4)(x_i - tE'_{k_0})^2/(\alpha^2 + itE''_{k_0}/2)}, \quad (5)$$

where we restored more generality [than in Eq. (4)] by using E'_{k_0} and E''_{k_0} to refer to the first and second derivatives of the dispersion E_k with respect to momentum k, and evaluated at k_0. For a quadratic dispersion one readily obtains the result Eq. (2). On the other hand, for the nearest neighbor model, $E'_{k_0} \equiv v_{k_0} = 2t_0 \sin(k_0)$ and $E''_{k_0} \equiv v'_{k_0} = 2t_0 \cos(k_0)$, where v_{k_0} is the group velocity and v'_{k_0} is the group velocity dispersion. The expansion is valid as long as $t \ll (\alpha/k_0)^3/t_0$. For $k_0 = \pi/2$, the validity length l is $l = v_{k_0} t \sim \alpha^3$. If α is on a nanometer scale, l is of order 1 μm.

We are now able to calculate the uncertainty relation for the lattice case with nearest neighbor hopping only, at any time t: $\langle x \rangle = 2t_0 \sin(k_0)t$ and $\langle x^2 \rangle = [2t_0 \sin(k_0)t]^2 + \alpha^2 + [t_0 \cos(k_0)t/\alpha]^2$. The uncertainty in position is then $\Delta x = \sqrt{\alpha^2 + t_0^2 \cos^2(k_0)t^2/\alpha^2}$. The uncertainty in the momentum is the same as in the continuum limit; namely, $\Delta k = 1/2\alpha$. Consequently, the uncertainty relation for this case on a lattice is

$$\Delta x \Delta k = \frac{1}{2}\sqrt{1 + \frac{t_0^2 \cos^2(k_0)t^2}{\alpha^4}}. \quad (6)$$

As one can see from this expression, in general the uncertainty never decreases as a function of time; the degree of increase depends on the mean momentum. However, if $k_0 = \pi/2$, the uncertainty remains unchanged. In other words, the wave packet possesses a solitonic behavior without showing the seemingly inevitable quantum spreading. We will demonstrate this fact numerically later. This possibility is actually well known in optics, where one seeks a medium with zero group velocity dispersion to minimize loss.[18] Nevertheless, this appears to be less appreciated in quantum mechanics.

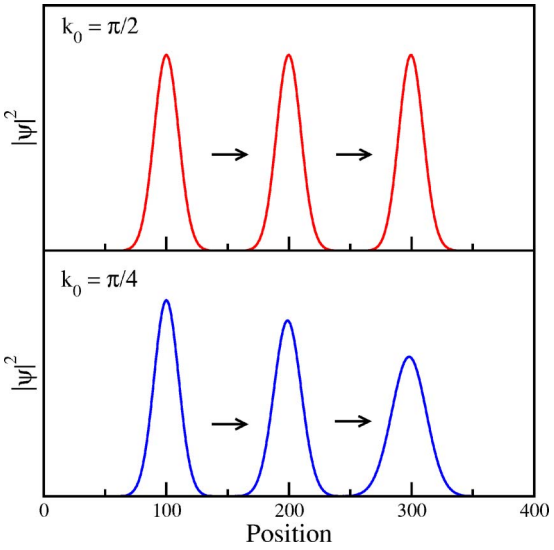

FIG. 1. (Color online) Time evolution of the wave packet with $k_0 = \pi/2$ (top) and $\pi/4$ (bottom). The wave packet with $k_0 = \pi/2$ does not spread while the wave packet $k_0 = \pi/2$ broadens as it moves.

This result persists in one dimension for any dispersion. That is, one can show that some wave vector always exists for which the group velocity dispersion is zero. In higher dimensions the situation is not quite as simple. The result remains for nearest neighbor hopping only. For example in three dimensions we have $E_k = -2t_0[\cos(k_x a) + \cos(k_y a) + \cos(k_z a)]$, and one readily obtains a similar result as in one dimension. However, when next nearest neighbor hopping is included, a little algebra shows that in general one cannot achieve conditions for zero group velocity dispersion.

To obtain this result numerically, one diagonalizes the tight-binding Hamiltonian $H_0 = -t_0 \Sigma_i (C_i^\dagger C_{i+1} + C_{i+1}^\dagger C_i)$ to obtain eigenvalues and the corresponding eigenstates. Then one can construct a wave packet, and evolve it in time according to the time-dependent Schrödinger equation (this procedure is described in more detail in Sec. IV). The result is plotted in Fig. 1 for three different times with $k_0 = \pi/2$ ($k_0 = \pi/4$) in the top (bottom) panel, respectively. A wave packet initially centered at $x_i = 100$ moves to $x_i \simeq 300$ in each panel. The uncertainty parameter α is set to be 10. The total time

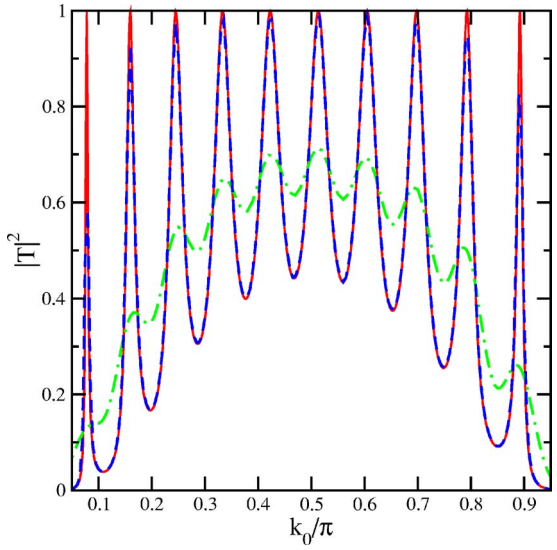

FIG. 2. (Color online) Transmission probability $|T|^2$ as a function of the mean momentum k_0 for $\alpha=6,60,\infty$. Two impurities with a potential $U=1$ are separated by ten lattice sites. The red solid curve is for a plane wave ($\alpha=\infty$). The blue dashed (green dot-dashed) curve is for a wave packet with $\alpha=60(6)$.

elapsed is different in the two panels because of the k_0 difference (in consistent dimensionless time units, 100 for the top, and 140 for the bottom panel). As one can see, the wave packet with $k_0=\pi/2$ does not spread and the peak height remains unchanged while the wave packet with $k_0=\pi/4$ spreads and the height becomes considerably smaller as it moves.

As shown earlier, the momentum uncertainty Δk is inversely proportional to α of a wave packet. It is worth checking to see how the plane wave result (for which $\Delta k=0$) is achieved, as α increases. We examine the case with static impurity scattering. For this we add, to H_0, impurity potential terms $\Sigma_{i\in\mathcal{I}}U_iC_i^\dagger C_i$, where U_i is a scalar potential at site i and $\mathcal{I}$ represents a set of impurities. Figure 2 illustrates the transmission probability as a function of the mean momentum k_0 of a wave packet for various α. We consider two impurities, each with a potential $U=1$, separated by 10 sites; thus, the impurity system spans 12 lattice sites. The red solid curve is for a plane wave ($\alpha=\infty$) while the blue dashed curve and the green dot-dashed curve are for a wave packet with $\alpha=60$ and 6, respectively. As Fig. 2 demonstrates, the wave packet approach will reproduce the plane wave results when α is much larger than the size of the impurity system. The same behavior holds in various other cases.

III. RESONANCE WIDTH FOR RANDOM TRIMERS

It is well known[20–23] now that correlated impurities allow extended electronic states for particular energy levels; thus, perfect transmission or resonance occurs. In this section we examine the width of the resonance for randomly distributed trimers as the number of trimers increases. The resonance width depicts the robustness of resonance for a change in the energy level.

Giri *et al.*[24] classified the parameter values for a trimer into five cases, for which perfect transmission can be obtained. The first is the dimer case, and the second only applies if the hopping parameters in the impurity region are different. We consider only the remaining three cases. Let us briefly describe the three cases using our notation. In case III, $U_0=U_1=U_2$ and perfect transmission occurs when $E=U_0\pm1$. This is the straightforward extension of the symmetric dimer case to a symmetric trimer, but note that now two solutions exist. In case IV, if $U_0+U_2=U_1$ then resonance is obtained at the energy, $E=U_1$ (we set the hopping parameter $t_0=1$), regardless of the values of U_0 and U_2. We will note an example below. In case V, $U_0=U_2$ and U_1 is arbitrary. The resonance is obtained for energies

$$E=U_1+\frac{1}{2}\left[U_1-U_0\pm\sqrt{(U_1-U_0)^2-4(U_1/U_0-2)}\right], \quad (7)$$

provided that $(U_1-U_0)^2\geq 4(U_1/U_0-2)$ and of course $-2\leq E\leq 2$.

For a trimer with U_0, U_1, and U_2 at sites $i=0$, 1 and 2, respectively, either the quantum mechanical approach (reviewed in Appendix A) or the transfer matrix formalism (see Appendix B) can be used to obtain the transmission amplitude as follows:

$$T=\frac{-2i\sin(k)}{(U_1-E_k)+e^{ik}[(U_0+U_2)(U_1-E_k)-2]+e^{2ik}[U_0U_2(U_1-E_k)-(U_0+U_2)]}. \quad (8)$$

We plot $|T|^2$ vs E for random trimers in Fig. 3. These results are obtained for a single trimer (smooth solid red curve) 50 trimers (blue curve, showing the most noise, and with intermediate width), and 500 trimers (green curve, with narrowest width in the four frames). In the latter two cases the trimers were randomly distributed in a one dimensional lattice, and an ensemble average over 50 different configurations was sampled. Figure 3(a) corresponds to case III with $U_0=U_1=U_2=0.5$. Figures 3(b) and 3(c) are for case (IV) $[U_0+U_2=U_1]$ with $U_0=0.6$ and $U_2=0.4$ and $U_0=0.9$ and $U_2=0.1$, respectively. Case V is illustrated in Fig. 3(d) with $U_0=U_2=0.6$ and $U_1=1$. As shown clearly in Fig. 3, the resonance width decreases considerably as the number of trimers increases for all three cases. For example, the resonance range around $E=0.5\pm1$ in Fig. 3(a) and around $E=1$ in Fig. 3(b) decreases significantly as the number of trimers increases up

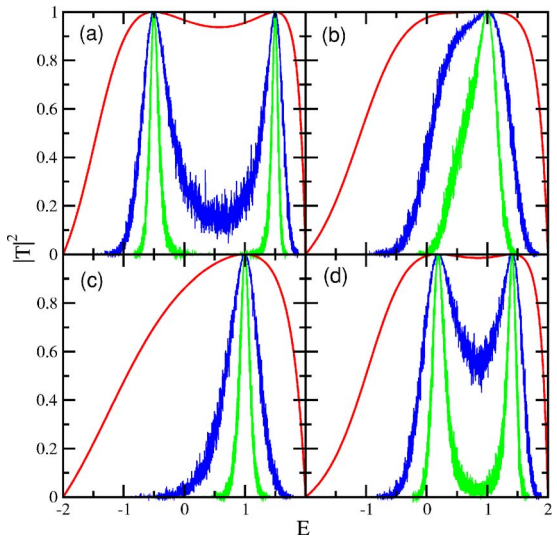

FIG. 3. (Color online) $|T|^2$ as a function of E for randomly distributed 50 impurity dimers (blue) and 500 dimers (green) in comparison with a single dimer (red). (a) corresponds to case III while (b) and (c) are for case IV, and (d) for case V.

to 500. Another interesting feature can be found in case IV.Even if the resonance occurs at $E=U_0+U_2$, a detailed characteristic of the resonance depends on values of $|U_0-U_2|$. For a given number of trimers, the resonance width decreases with increasing $|U_0-U_2|$. One can see this by comparing the results in Figs. 3(b) and 3(c).

IV. NUMERICAL DIAGONALIZATION AND PHASE SHIFT OF WAVE PACKETS

We have already alluded to the numerical approach for a free wave packet transfer in Sec. II. Since the operator $C_i^\dagger$ creates an electron at site i, the initial wave packet can be written as $|\psi(0)\rangle=\Sigma_i\varphi(x_i,0)C_i^\dagger|0\rangle$, where

$$\varphi(x_i,0)=\frac{1}{(2\pi a^2)^{1/4}}e^{ik_0(x_i-x_0)}e^{-(1/4)(x_i-x_0)^2/\alpha^2}. \tag{9}$$

As mentioned in Sec. II, x_0 is the mean position, k_0 is the mean momentum, and α is the initial uncertainty associated with the position. If α is much larger than the size of the potential region, say I, the wave packet acts like a plane wave when it is scattered off the potential. To see the real time propagation of a wave packet in a lattice with N_0 sites in total, one needs to diagonalize the Hamiltonian Eq. (A1), which is an $(N_0\times N_0)$ matrix. Since the impurity potentials are real, the Hamiltonian matrix is real and symmetric. The numerical diagonalization is done using the expert driver DSYEVX contained in the LAPACK package, which provides either selected eigenvalues and eigenvectors or the entire spectrum. Using the eigenstates $|n\rangle$ and eigenvalues ϵ_n obtained from the diagonalization, one can express the wave packet at time t as follows:

$$|\psi(t)\rangle=\sum_{n=1}^{N_0}|n\rangle\langle n|\psi(0)\rangle e^{-i\epsilon_n t}. \tag{10}$$

The wave packet initially at x_0 moves towards the potentials and scatters off impurities. In general, the wave packet is partially reflected and partially transmitted. The mathematical definitions of the reflection and transmission probabilities are $|R|^2=\Sigma_{i<0}|\varphi(x_i,t)|^2$ and $|T|^2=\Sigma_{i>I}|\varphi(x_i,t)|^2$, respectively, as $t\to\infty$.

Let us consider the two-impurity case again to illustrate the time evolution of a wave packet in the presence of impurities in a lattice. The impurity potentials are set to be $U_0=1$ and $U_1=3$ in units of the hopping constant t_0. We consider wave packets with average momentum that varies from $k_0=0.3\pi$ to 0.9π. The time elapsed for the scattering processes to "finish" depends on k_0; for example, for $k_0=0.6\pi$ it is 160 in our dimensionless time unit, while for $k_0=0.8\pi$, it would be 240. We consider two impurity configurations, I and II. For I, we have (U_0,U_1) and for II, (U_1,U_0). As we discussed earlier, the reflection amplitude will differ correspondingly; namely, R for I while R' for II. Since $T=T'$, there is no phase shift for the transmitted wave packet as shown in Ref. 20. On the other hand, the phase difference δ induces the phase shift for the reflected wave packets. This can be explained as follows. Consider a wave packet $\psi(x,0)$ moving with k_0 to an impurity region

$$\psi(x,0)=\int dk\, g(k)e^{ik_0(x-x_0)} \tag{11}$$

where $g(k)\sim e^{-\alpha(k-k_0)^2}$. After the wave packet scatters completely off the impurities at time t_s, the wave function at t after t_s would be

$$\psi_{[I]}(x,t)=\int dk\, g_R(k)e^{-ik_0(x-x_R)}e^{-iE_k t}+\int dk\, g_T(k)e^{ik_0(x-x_T)}e^{-iE_k t}, \tag{12}$$

where an elastic scattering is assumed, $g_R\sim R(k)g(k)$ while $g_T\sim T(k)g(k)$, and $x_R(x_T)$ is the mean position of the reflected (transmitted) wave packet at t_s. For the reverse configuration II,

$$\psi_{II}(x,t)=\int dk\, g_{R'}(k)e^{-ik_0(x-x_R)}e^{-iE_k t}+\int dk\, g_{T'}(k)e^{ik_0(x-x_T)}e^{-iE_k t}. \tag{13}$$

Since $R'=Re^{i\delta}$, the reflected part of $\psi_{II}(x,t)$ becomes

$$\psi_{II,R}(x,t)\sim\int dk\, R(k)e^{-\alpha(k-k_0)^2}e^{-ik_0(x-x_R)-iE_k t+i\delta}. \tag{14}$$

In order to see the phase shift of the reflected wave packets, one needs to calculate $|\psi_{II,R}|^2$. Expanding $E(k)$ and $\delta(k)$ around k_0 and some algebra yields

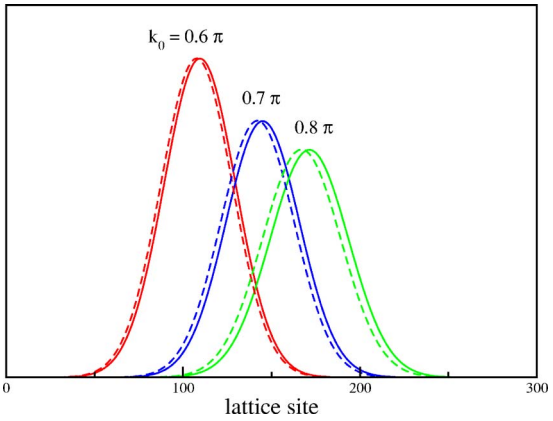

FIG. 4. (Color online) Phase shift of the reflected wave packets in a lattice with two impurities embedded side by side with $U_0=1$ and $U_1=3$ in units of the hopping constant. Initially, the wave packet is at $x_0=150$. The two impurities are at 300 and 301. The uncertainty parameter α is set to be 20. For $|\psi_{I,R}|^2$ (solid curves), the impurity configuration is (U_0,U_1) while for $|\psi_{II,R}|^2$ (dashed curves), it is (U_1,U_0).

$$|\psi_{II,R}|^2 \sim \exp\left(-\frac{(x-x_R+v_0t-\partial_k\delta_0)^2}{2\{\alpha^2+t^2(\partial_k^2E_0-\partial_k^2\delta_0)^2/4\}}\right), \quad (15)$$

where $v_0=\partial_kE_0$. Rigorously speaking, this approximation is valid when $R(k)\simeq R(k_0)$. Note that the term with E_0 and δ_0 disappears when $|\psi_{II,R}|^2$ is calculated and the position of the scattered wave is x_R-v_0t. Equation (15) indicates that the phase shift of the reflected wave packets is determined by $\partial_k\delta_0$, and the spreading depends not only on $\partial_k^2E_0$ but also on $\partial_k^2\delta_0$. To be specific we define a phase shift as the difference between the two reflected wave packets for configurations I and II at their half-width as in Ref. 20.

In Fig. 4, we plot the reflected wave packets for I (solid curves) and II (dashed curves) in the case of two impurities with $U_0=1$ and $U_1=3$. The average momenta for the three wave packets shown are $k_0=0.6\pi$, 0.7π, and 0.8π. As one can see clearly, the phase shift between $|\psi_{I,R}|^2$ (solid curves) and $|\psi_{II,R}|^2$ (dashed curves) depends on k_0. The phase shift for $k_0=0.6\pi$ is not significant while it becomes bigger as k_0 increases to 0.8π. We also plot the phase difference, its derivative, and the phase shift of the reflected wave packets in Fig. 5. As shown in the plot, the derivative of δ and the phase shift obtained numerically are in excellent agreement.

V. SPIN-FLIP SCATTERING

So far we have discussed scalar potential scattering on a lattice. In this section we describe how to study spin-flip scattering on a lattice. Let us consider the Hamiltonian

$$H=-t_0\sum_{\langle i,j\rangle\sigma}C_{i\sigma}^\dagger C_{j\sigma}-2J_0\sum_l \sigma_l\cdot\mathbf{S}_l-2J_1\sum_l \mathbf{S}_l\cdot\mathbf{S}_{l+1} \quad (16)$$

where $C_{i\sigma}^\dagger$ creates an electron with a spin σ at a site i, $\mathbf{S}_l$ is a spin operator located at site l, t_0 is the hopping amplitude between the nearest neighbor sites, and J_0 is the coupling

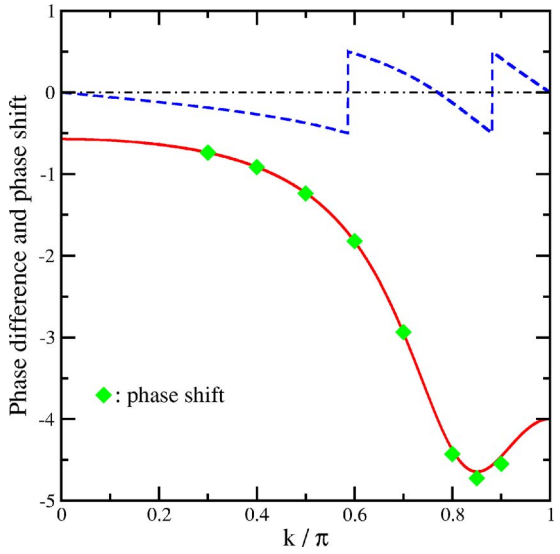

FIG. 5. (Color online) Phase difference (blue dashed curve), its derivative (red solid curve), and the phase shift obtained from the wave packet simulations (green diamond symbols). The phase shift is measured by the difference between the reflected wave packets $\psi_{I,R}|$ and $\psi_{II,R}|$ at their half-width. The impurity potentials are $U_0=1$ and $U_1=3$. The phase shift and $\partial\delta/\partial k$ agree with one another very well.

between an electron and a local spin. The electron-spin coupling is assumed here to be a purely local (i.e., on-site) interaction between the electron spin σ_l at site l, and the local spin at site l, denoted by S_l. J_1 is the (Heisenberg exchange) coupling between two neighboring spins. This model can be used to understand the spin transfer dynamics between an itinerant electron and a ferromagnetic spin chain with N_s local spins $(S=1/2)$ arranged in a one-dimensional lattice. To study the spin chain, one can extend the quantum mechanical approach as in Ref. 14, or one can extend the transfer matrix formalism.[27] Here we follow the diagonalization method to see the time evolution of the spins.

Suppose we send a wave packet representing an electron with spin aligned in the $+Z$ direction toward a ferromagnetic spin chain where all spins are aligned in the $-Z$ direction. Such a state of the chain will be denoted by $|G\rangle$. The incoming wave packet can be constructed as follows:

$$|\psi(0)\rangle=\sum_i \varphi(x_i,0)C_{i\uparrow}^\dagger|0\rangle. \quad (17)$$

Then, the initial wave function of the total system including the incoming electron and the chain is $|\psi(0)\rangle=|\psi(0)\rangle|G\rangle$. We introduce the total spin operator $\mathbf{J}=\sigma+\Sigma_l\mathbf{S}_l$. The Z component J_z of the total spin is conserved. Hereafter we assume spin 1/2 for both the electron and the spins, for simplicity. Since the initial value of J_z is $(1-N_s)/2$, the possible spin bases would be $|+\rangle|G\rangle$ and $|-\rangle S_{l+}|G\rangle$, where S_{l+} flips the local spin at l in the chain. Alternative spin bases could be used by utilizing the total spin and its Z component. Including the location of the incoming electron, the basis states we use are $C_{i\uparrow}^\dagger|0\rangle|G\rangle$ and $C_{i\downarrow}^\dagger|0\rangle S_{l+}|G\rangle$. Now, the Hamiltonian becomes an $N_0(N_s+1)\times N_0(N_s+1)$ matrix. Note that the di-

mension of the Hamiltonian depends only on N and N_s and does not depend on the locations of the local spins. Even if we include impurities, the dimension of the Hamiltonian remains unchanged. To construct the Hamiltonian matrix, we need to calculate each component of the matrix. For example,

$$\langle G|\langle 0|C_{j\uparrow}(-2J_0\boldsymbol{\sigma}_l\cdot\mathbf{S}_l)C_{i\uparrow}^{\dagger}|0\rangle|G\rangle=\frac{J_0}{2}\delta_{j,l}\delta_{i,l},$$

$$\langle G|\langle 0|C_{j\uparrow}(-2J_1\mathbf{S}_l\cdot\mathbf{S}_{l+1})C_{i\uparrow}^{\dagger}|0\rangle|G\rangle=-\frac{J_1}{2}\delta_{i,j}.$$

Other components for the Hamiltonian matrix are presented in Appendix C.

We therefore solve the eigenvalue problem $H|\eta_j\rangle=E_j|\eta_j\rangle$, where $j=1,2,\ldots,N_0(N_s+1)$. Then, we represent the time-dependent total state using eigenvalues and eigenstates as follows: $|\psi(t)\rangle=\Sigma_j|\eta_j\rangle\langle\eta_j|\psi(0)\rangle e^{-iE_jt}$. Alternatively, the total state at t can be expressed as

$$|\psi(t)\rangle=\sum_{i=1}^{N_0}\psi_i(t)C_{i\uparrow}^{\dagger}|0\rangle|G\rangle+\sum_{l=1}^{N_s}\sum_{i=1}^{N_0}\psi_{l,i}(t)C_{i\downarrow}^{\dagger}|0\rangle S_{l+}|G\rangle, \tag{18}$$

where $|\psi_i(t)|^2$ is the probability to find an electron with spin up at site i while the local spins are all pointing down at time t, and $|\psi_{l,i}(t)|^2$ is the probability for the electron with spin down at site i while the lth local spin is pointing up and the others pointing down at time t. Using this expression we can investigate the dynamics of a particular spin or the sum of all spins in the chain. For example,

$$\langle\psi(t)|S_{lz}|\psi(t)\rangle=-\frac{1}{2}\sum_{i'}|\psi_{i'}|^2+\frac{1}{2}\sum_{l',i'}|\psi_{l',i'}|^2(2\delta_{l,l'}-1), \tag{19}$$

and the total local spin is $\Sigma_l\langle\mathbf{S}_l(t)\rangle$. Since at $t=0$, $\psi_{l,i}=0$ and $\Sigma_i|\psi_i|^2=1$, $\langle S_{lz}(0)\rangle=-1/2$ is assumed. Thus, $\langle S_z(0)\rangle=\Sigma_l\langle S_{lz}(0)\rangle=-N_s/2$ and $\langle J_z(0)\rangle=(1-N_s)/2$.

By way of an example, consider a chain of three spins, ferromagnetically coupled with strength J_1. As an electron impinges on the three spin system, they interact with the electronic spin and change their states. In Fig. 6, we first plot the expectation value of S_z for $\mathbf{S}_i$ $(i=1,2,3)$, and $\mathbf{S}_{tot}=\Sigma_{i=1}^{3}\mathbf{S}_i$ for the uncoupled spin case, i.e., with $J_1=0$. The electron is coupled to each spin with strength $J_0=2$, in units of t_0. Since there is no coupling between two nearest spins in this instance, each spin evolves independently as a function of time. The spin transfer from the incoming electron to the local spins occurs mostly for $\mathbf{S}_1$ while it is minimal for $\mathbf{S}_3$.

On the other hand, when the spins are Heisenberg coupled with strength $J_1=1$ all three spins participate in the spin-flip scattering with the incoming electron almost to the same degree, as shown in Fig. 7. Interestingly, even though there is an obvious asymmetry (the electron strikes the first spin first) the time evolutions of the first (S_1) and the third (S_3) spins are almost identical.

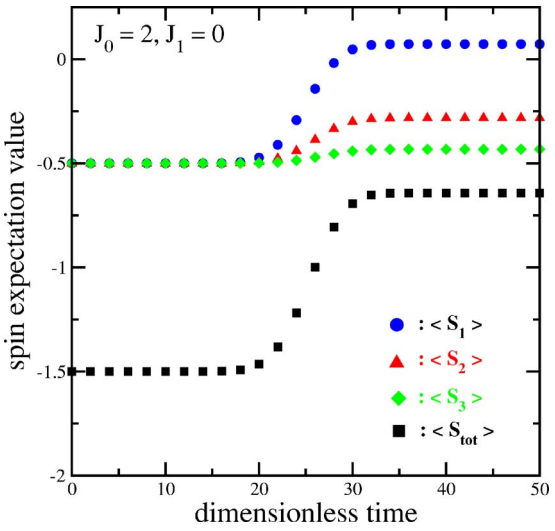

FIG. 6. (Color online) The spin expectation value $\langle S_z\rangle$ for three spins S_i $(i=1,2,3)$ and the total spin S_{tot}. The coupling parameters are $J_0=2$ and $J_1=0$.

VI. CONCLUSIONS

In this paper we have described scattering of a wave packet in a lattice. One of its interesting natures is a possible solitonic behavior of a wave packet which is impossible in continuous media. We examined several examples of impurity scattering. In particular, we explored the robustness of the resonance for randomly distributed trimers as their number increases. We found that the resonance width decreases as the number of trimers increases.

Numerical diagonalization has been used for solution of completely general problems, including those involving spin-flip scattering, as explored briefly in the last section. Using the diagonalization, one can monitor the time dependence of the wave function amplitudes throughout the scattering event. This will be of interest as experimental methods

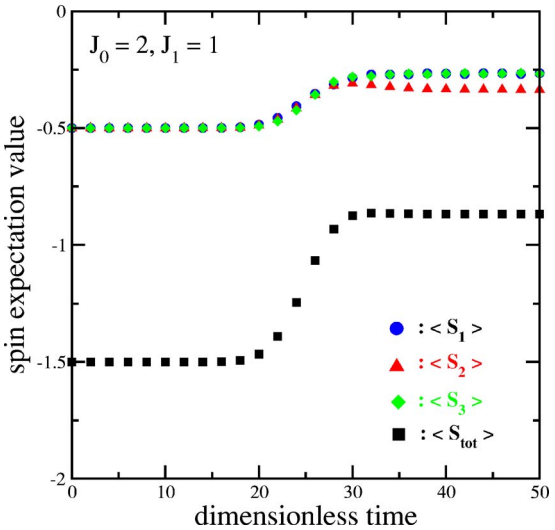

FIG. 7. (Color online) The spin expectation value $\langle S_z\rangle$ for three spins S_i $(i=1,2,3)$ and the total spin S_{tot}. The coupling parameters are $J_0=2$ and $J_1=1$.

evolve to allow more controlled temporally and spatially resolved measurements. We presented, by way of example the case of a Heisenberg chain of spins, interacting with an itinerant electron (spin current). A natural extension of this calculation could be to include more spins, so as to model an actual magnetized thin film. Generalizing to the case of a spin current is straightforward, so long as we assume the electrons in the current do not interact with one another. This will allow us to address detailed questions about how the spins in the chain reverse their magnetization when subjected to a spin current. These and other questions will be the subject of future investigation.

ACKNOWLEDGMENTS

We wish to thank J. Hirsch for early correspondence concerning the solution of the Schrödinger equation as presented in Ref. 19. W.K. acknowledges A. Mann and M. Revzen for helpful discussions. This work was supported in part by the Natural Sciences and Engineering Research Council of Canada (NSERC), by ICORE (Alberta), and by the Canadian Institute for Advanced Research (CIAR). F.M. is appreciative of the hospitality of the Department of Condensed Matter Physics at the University of Geneva.

APPENDIX A: QUANTUM MECHANICAL APPROACH

Electronic transfer through impurities on a lattice can be explored in one of three ways: either through a quantum mechanical approach using matching conditions of wave functions, or through the transfer matrix formalism, or through direct diagonalization of the Hamiltonian. We provide summaries of the first two approaches in this appendix and the next, respectively. Note that if there are N impurities embedded in a lattice, one needs to deal with a $(2N\times 2N)$ matrix to determine all the relevant coefficients including R and T in the quantum mechanical approach. On the other hand, the transfer matrix formalism requires manipulation of N (2×2) matrices.

In a lattice, a potential is represented by a series of "impurities" whose effect is to alter the on-site energy wherever an impurity has substituted for the usual atom. This is represented by the Hamiltonian,

$$H = -t_0 \sum_i [C_i^\dagger C_{i+1} + C_{i+1}^\dagger C_i] + \sum_{i\in\mathcal{I}} U_i C_i^\dagger C_i, \qquad \text{(A1)}$$

where t_0 is the hopping amplitude as before, $C_i^\dagger$ creates an electron at site i, and U_i is a scalar potential at site i; the set of impurities spans a number $\mathcal{I}=\{0,1,2,\ldots,I\}$. The wave function defined only on the lattice sites can now be written as a piecewise function over $I+3$ regions if the number of impurities is $I+1$. That is, $|\psi\rangle=\Sigma_j \psi(x_j) C_j^\dagger |0\rangle$, where

$$\psi(x_j) = \begin{cases} \psi_L(x_j) = e^{ikx_j} + Re^{-ikx_j} & \text{for } j<0, \\ \psi_j(x_j) = A_j e^{iq_j x_j} + B_j e^{-iq_j x_j} & \text{for } j\in\mathcal{I}, \\ \psi_R(x_j) = Te^{ikx_j} & \text{for } j>I, \end{cases}$$

and $|0\rangle$ represents the vacuum, namely, the state with an empty lattice. The coefficients R, A_i, B_i, and T are to be determined by matching conditions at $i\in\mathcal{I}$. Note that q_i will be obtained within the same calculation even though we can already guess that $E_k=E_{q_i}+U_i$. What are the matching conditions? As in the continuum limit one first demands continuity of the wave function at each site. Therefore, $\langle 0|C_{j+}|\psi\rangle=\langle 0|C_{j-}|\psi\rangle$, where $j+$ $(j-)$ means just to the right (left) of site j. However, the second condition in the continuum limit requires continuity of the *derivative* of the wave functions at each site. One can see this directly from the Schrödinger equation through an integration of the second-order differential equation. However, the second quantized form of the Hamiltonian written in Eq. (A1) contains no derivatives, so clearly this procedure is not an option. The correct procedure is as follows.[19] One first writes down the Schrödinger equation projected onto each site, $\langle 0|C_j H|\psi\rangle = \langle 0|C_j E|\psi\rangle$ for $j=0,1,\ldots,I$. Then the two conditions, expressed for each site, can be written

$$\psi(j+0^+) = \psi(j+0^-), \qquad \text{(A2)}$$

$$-t_0[\psi(j+1)+\psi(j-1)] + U_j\psi(j) = E\psi(j). \qquad \text{(A3)}$$

As mentioned before, Eq. (A2) implies that the wave function is continuous at each site. Equation (A3) is the Schrödinger equation at each site; however, close inspection shows that on the left-hand side the wave function is required from two different "pieces" in the domain (assuming that U_j is nonzero). But we would like the Schrödinger equation for noninteracting electrons to be satisfied, with the same eigenvalue, by the wave function on any given piece even when extended beyond the domain of validity of that wave function. For example, for $j=0$ we demand that ψ_L satisfy the equation $-t_0[\psi_L(+1)+\psi_L(-1)]=E\psi_L(0)$. Note that we have used the wave function ψ_L at location +1, even though it was originally defined only for sites 0 or below. Moreover, we require that this equation be satisfied with the same eigenvalue E. Hence, by judicious adding and subtracting of a wave function to Eq. (A3) at each impurity site, we arrive at, for $j=0$ and $j=I$,

$$-t_0\psi_1(1) + t_0\psi_L(1) + U_0\psi_L(0) = 0 \quad \text{for } j=0, \qquad \text{(A4)}$$

$$-t_0\psi_I(I-1) + t_0\psi_R(I-1) + U_I\psi_R(I) = 0 \quad \text{for } j=I. \qquad \text{(A5)}$$

Similar equations apply for the impurity sites in between. These can now be solved for the unknown coefficients along with the matching equations [Eq. (A2)].

Let us consider a two-impurity case as an example. Assume that two impurities with U_0 and U_1 are embedded at $j=0$ and 1, respectively, in a lattice; one needs to introduce a wave function as follows:

$$\psi(x_j) = \begin{cases} \psi_L(x_j) = e^{ikx_j} + Re^{-ikx_j}, \\ \psi_0(x_j) = A_0 e^{iq_0 x_j} + B_0 e^{-iq_0 x_j}, \\ \psi_1(x_j) = A_1 e^{iq_1 x_j} + B_1 e^{-iq_1 x_j}, \\ \psi_R(x_j) = Te^{ikx_j}. \end{cases}$$

The coefficients such as R and T and the momenta q_0 and q_1 can be determined by solving the continuity equations $\psi_L($

$-1)=\psi_1(-1)$, $\psi_L(0)=\psi_1(0)$, $\psi_1(0)=\psi_2(0)$, $\psi_1(1)=\psi_2(1)$, $\psi_2(1)=\psi_R(1)$, $\psi_1(2)=\psi_R(2)$, and the Schrödinger equations

$$-\psi_1(1)+\psi_L(1)+U_0\psi_L(0)=0,$$

$$-\psi_1(0)+\psi_R(0)+U_1\psi_R(1)=0, \tag{A6}$$

where we set the nearest neighbor hopping amplitude t_0 to be unity for simplicity. It is straightforward to show that

$$T=\frac{2i\sin(k)}{2i\sin(k)-(U_0+U_1)-U_0U_1e^{ik}}, \tag{A7}$$

$$R=\frac{U_0+U_1e^{2ik}+U_0U_1e^{ik}}{2i\sin(k)-(U_0+U_1)-U_0U_1e^{ik}}. \tag{A8}$$

Using the Schrödinger equations, one can show that $E_k=E_{q_i}+U_i$ $(i=1,2)$. This result will be used to compare the quantum mechanical approach and the transfer matrix formalism. The case of two impurities with the same potential $(U_0=U_1)$ has been well studied in the context of the random dimer model.[21–23]

APPENDIX B: TRANSFER MATRIX FORMALISM

In the transfer matrix formalism,[25] we write the Schrödinger equation (A3) in the matrix form as follows:

$$\begin{pmatrix}\psi_{j+1}\\ \psi_j\end{pmatrix}=M_j\begin{pmatrix}\psi_j\\ \psi_{j-1}\end{pmatrix} \tag{B1}$$

where $M_j=\begin{pmatrix}U_j-E_k & -1\\ 1 & 0\end{pmatrix}$, which is a unimodular matrix and associated with an impurity at the site j. The wave functions ψ_L (for $i<1$) and ψ_R (for $i>N$) are $\psi_L=e^{ikx_i}+Re^{-ikx_i}$ and $\psi_R=Te^{ikx_i}$. Using the transfer matrix formalism, one can express the coefficients R and T in terms of k, U_i, and E as follows:

$$\begin{pmatrix}\mathcal{T}\\ i\mathcal{T}\end{pmatrix}=P\begin{pmatrix}1+\mathcal{R}\\ i(1-\mathcal{R})\end{pmatrix}, \tag{B2}$$

where $P=S^{-1}MS$ with $S=\begin{pmatrix}\cos(k) & \sin(k)\\ 1 & 1\end{pmatrix}$, and $M=M_NM_{N-1}\cdots M_1$. Solving Eq. (B2), one can obtain[26]

$$\mathcal{T}=\frac{2i}{i(P_{11}+P_{22})+P_{12}-P_{21}}, \tag{B3}$$

$$\mathcal{R}=\frac{P_{12}+P_{21}-i(P_{11}-P_{22})}{i(P_{11}+P_{22})+P_{12}-P_{21}}. \tag{B4}$$

It is instructive to compare the quantum mechanical approach and the transfer formalism using an example. Let us again consider two impurities residing side by side. In this instance we know that the transmission and reflection amplitude are Eqs. (A7) and (A8). In the transfer matrix formalism, one needs to calculate $P=S^{-1}M_1M_0S$ to obtain the transmission amplitude

$$\mathcal{T}=\frac{2i\sin(k)}{i\sin(k)[(U_0-E_k)(U_1-E_k)-2]+U_0+U_1-2E_k-\cos(k)(U_0-E_k)(U_1-E_k)}. \tag{B5}$$

Note that T [Eq. (A7)] is not identical with $\mathcal{T}$ [Eq. (B5)]. However, while this is not obvious, they merely differ by a phase factor and their magnitudes are the same: $\mathcal{T}=e^{2ik}T$. Clearly the transfer matrix method "keeps track" of the two lattice spacings traversed as the particle is transmitted to the other side. A similar relation holds for the reflection amplitude. Consequently, the transmission (reflection) probabilities are identical; $|T|^2=|\mathcal{T}|^2$ and $|R|^2=|\mathcal{R}|^2$ in the two formalisms.

In previous work[20] using the transfer matrix formalism, we derived a relation between $\mathcal{R}$ and $\mathcal{R}'$, where $\mathcal{R}'$ is the reflection amplitude for the reverse impurity configuration. It is

$$\frac{\mathcal{T}^*(\mathcal{R}'-\mathcal{R})}{\mathcal{T}(\mathcal{R}'-\mathcal{R})^*}=e^{2ik}. \tag{B6}$$

In the example of the two impurities, $\mathcal{R}'$ is given by $\mathcal{R}$ with U_0 and U_1 exchanged. Using Eqs. (A7) and (A8), one can show that T and R also satisfy the same relation; namely,

$$\frac{T^*(R'-R)}{T(R'-R)^*}=e^{2ik}. \tag{B7}$$

Introducing a phase difference between R and R' such as $R'=e^{\delta}R$, we obtain

$$e^{i\delta}=-e^{2ik}\frac{R^*T}{RT^*}. \tag{B8}$$

APPENDIX C: COMPONENTS OF THE HAMILTONIAN MATRIX FOR A SPIN CHAIN

Other components one needs to construct the Hamiltonian matrix are the following:

$$\langle G|\langle 0|C_{j\uparrow}\left(-t_0\sum_{i'\sigma}(C^{\dagger}_{i'+1,\sigma}C_{i'\sigma}+\mathrm{H.c.})\right)C^{\dagger}_{i\uparrow}|0\rangle|G\rangle = -t_0\delta_{j,i+1}-t_0\delta_{j+1,i}, \tag{C1}$$

$$\langle G|S_{l-}\langle 0|C_{j\downarrow}\left(-t_0\sum_{i'\sigma}(C^{\dagger}_{i'+1,\sigma}C_{i'\sigma}+\mathrm{H.c.})\right)C^{\dagger}_{i\downarrow}|0\rangle S_{l+}|G\rangle = -t_0\delta_{j,i+1}-t_0\delta_{j+1,i}, \tag{C2}$$

$$\langle G|\langle 0|C_{j\uparrow}(-2J_0\sigma_l\cdot\mathbf{S}_l)C^{\dagger}_{i\downarrow}|0\rangle S_{l'+}|G\rangle = -J_0\delta_{l,l'}\delta_{j,l}\delta_{i,l}, \tag{C3}$$

$$\langle G|S_{l'-}\langle 0|C_{j\downarrow}(-2J_0\sigma_l\cdot\mathbf{S}_l)C^{\dagger}_{i\downarrow}|0\rangle S_{l'+}|G\rangle = J_0\left(\delta_{l,l'}-\frac{1}{2}\right)\delta_{j,l}\delta_{i,l}, \tag{C4}$$

$$\langle G|S_{l''-}\langle 0|C_{j\downarrow}(-2J_1\mathbf{S}_l\cdot\mathbf{S}_{l+1})C^{\dagger}_{i\downarrow}|0\rangle S_{l'+}|G\rangle = -J_1\delta_{i,j}\left[2\left(\delta_{l+1,l'}-\frac{1}{2}\right)\left(\delta_{l,l'}-\frac{1}{2}\right)\delta_{l'',l'}+\delta_{l'',l}\delta_{l+1,l'}+\delta_{l'',l+1}\delta_{l,l'}\right]. \tag{C5}$$

[1] M. Drescher, M. Hentschel, R. Kienberger, M. Uiberacker, V. Yakovlev, A. Scrinzi, Th. Westerwalbesloh, U. Kleineberg, U. Heinzmann, and F. Krausz, Nature (London) **419**, 803 (2002).

[2] A. Baltuka, Th. Udem, M. Uiberacker, M. Hentschel, E. Goulielmakis, Ch. Gohle, R. Holzwarth, V. S. Yakovlev, A. Scrinzi, T. W. Hansch, and F. Krausz, Nature (London) **421**, 611 (2003).

[3] F. A. Hegmann, Phys. Canada **59**, 127 (2003).

[4] M. R. Freeman and W. K. Hiebert, in *Spin Dynamics in Confined Magnetic Structures I*, edited by B. Hillebrands and K. Ounadjela (Springer, Berlin, 2002).

[5] B. C. Choi, M. Belov, W. K. Hiebert, G. E. Ballentine, and M. R. Freeman, Phys. Rev. Lett. **86**, 728 (2001).

[6] See, for example, P. A. Rikvold, G. Brown, S. J. Mitchell, and M. A. Novotny, in *Nanostructured Magnetic Materials and their Applications*, edited by D. Shi, B. Aktas, L. Pust, and F. Mikailov, Springer Lecture Notes in Physics Vol. 593 (Springer, Berlin, 2002), p. 164; see also cond-mat/0110103 (unpublished).

[7] L.-C. Ku and S. A. Trugman, cond-mat/0310226 (unpublished).

[8] L. Berger, Phys. Rev. B **54**, 9353 (1996).

[9] J. C. Slonczewski, J. Magn. Magn. Mater. **159**, L1 (1996).

[10] J. C. Slonczewski, J. Magn. Magn. Mater. **195**, L261 (1999).

[11] L. Berger, J. Appl. Phys. **89**, 5521 (2001).

[12] J. Z. Sun, Phys. Rev. B **62**, 570 (2000).

[13] J. Miltat, G. Albuquerque, and A. Thiaville, in *Spin Dynamics in Confined Magnetic Structures I*, edited by B. Hillebrands and K. Ounadjela (Springer, Berlin, 2002).

[14] W. Kim and F. Marsiglio, Europhys. Lett. **69**, 595 (2005).

[15] W. Kim and F. Marsiglio, Phys. Rev. B **69**, 212406 (2004).

[16] M. D. Stiles and A. Zangwill, Phys. Rev. B **66**, 014407 (2002).

[17] See, for example, R. Shankar, *Principles of Quantum Mechanics* (Plenum Press, New York, 1980).

[18] See, for example, G. P. Agrawal, *Nonlinear Fiber Optics* (Academic Press, New York 2001). We thank F. Hegmann for pointing this out to us.

[19] J. E. Hirsch, Phys. Rev. B **50**, 3165 (1994).

[20] W. Kim, L. Covaci, and F. Marsiglio, Phys. Rev. B **73**, 195109 (2006).

[21] D. H. Dunlap, H.-L. Wu, and P. W. Phillips, Phys. Rev. Lett. **65**, 88 (1990).

[22] H.-L. Wu and P. Phillips, Phys. Rev. Lett. **66**, 1366 (1991).

[23] H.-L. Wu, W. Goff, and P. Phillips, Phys. Rev. B **45**, 1623 (1992).

[24] D. Giri, P. K. Datta, and K. Kundu, Phys. Rev. B **48**, 14113 (1993).

[25] For an excellent discussion on the continuum limit, see R. Gilmore, *Elementary Quantum Mechanics in One Dimensions* (The Johns Hopkins University Press, Baltimore, MD, 2004).

[26] B. L. Burrows and K. W. Sulston, Phys. Rev. B **51**, 5732 (1995).

[27] Y. Avishai and Y. Tokura, Phys. Rev. Lett. **87**, 197203 (2001).